

Microscale inverse acoustic band gap structure in aluminum nitride

Nai-Kuei Kuo,^{a)} Chengjie Zuo,^{a)} and Gianluca Piazza^{a)}

Department of Electrical and Systems Engineering, University of Pennsylvania, Philadelphia, Pennsylvania 19104, USA

(Received 9 June 2009; accepted 6 August 2009; published online 2 September 2009)

This work presents the design and demonstration of a microscale inverse acoustic band gap (IABG) structure in aluminum nitride (AlN) with a frequency stop band for bulk acoustic waves in the very high frequency range. Conversely to conventional microscale acoustic band gaps, the IABG is formed by a two-dimensional periodic array of unit cells consisting of a high acoustic velocity material cylinder surrounded by a low acoustic velocity medium. The periodic arrangement of the IABG array induces scattering of incident acoustic waves and generates a stop band, whose center frequency is primarily determined by the lattice constant of the unit cell and whose bandwidth depends on the cylinder radius, the film thickness, and the size of the tethers that support the cylinder. A wide band gap ($>13\%$ of the center frequency) is formed by the IABG even when thin AlN films are used. The experimental response of an IABG structure having a unit cell of $8.6 \mu\text{m}$ and an AlN film thickness of $2 \mu\text{m}$ confirms the existence of a frequency band gap between 185 MHz and 240 MHz. © 2009 American Institute of Physics. [DOI: 10.1063/1.3213345]

Emerging phononic crystal (PC) based applications in the area of ultrasonic transducers and radio frequency (rf) communication and potential integration of PCs with microelectromechanical systems (MEMS) devices (such as in PC-based resonators) have spurred recent research interest in microscale PCs.^{1,2} PCs, which are also known as acoustic band gap (ABG) structures, are characterized by a periodic cell arrangement with mismatch in the acoustic properties (i.e., density and elastic constant) of the materials that form it. The periodic nature and the acoustic mismatch of the ABG induce phonon scattering within the array and prohibit the propagation of acoustic waves at specific wavelengths, which are determined by the physical parameters of the unit cell such as the lattice constant, a , the radius of the inclusion, r , and the thickness, d .^{3,4} The range of the rejected acoustic waves is known as the frequency band gap. Most of the current work on microscale ABGs has been focusing on maximizing the size of the frequency band gap and increasing the frequency of operation. Few research groups have investigated and demonstrated bulk wave ABG structures in the very high frequency (VHF) range.^{5,6} The ABG design of these previous demonstrations is based on a conventional cell arrangement having a high acoustic velocity matrix with low acoustic velocity inclusions. Recent work from Mohammadi *et al.*⁵ has shown that the use of a hexagonal lattice in silicon generates a wider complete band gap in comparison to a square lattice. However, in order to induce a sufficiently wide frequency band gap, the hexagonal lattice requires the film thickness to be approximately the same of the lattice constant ($d/a \sim 1$). This solution imposes significant challenges in the making of the ABG structure and limits the direct in-plane integration of the ABG with bulk electroacoustic devices in the VHF range, which generally require the film thickness to be $1\text{--}2 \mu\text{m}$.⁷

This work introduces a distinct class of ABG structures that relaxes the restriction on the film thickness and simultaneously attains wide band gaps in the VHF range. This design is called the inverse ABG (IABG) structure. Differently from the conventional ABG structures, the IABG inverts the acoustic velocity distribution in a unit cell by having the high acoustic velocity material in the center surrounded by a low acoustic velocity medium. The material in the center is suspended by four thin tethers [Fig. 1(b)]. In this configuration, the width of the frequency band gap depends not only on the conventional geometrical parameters (a , r , and d), but also on an additional parameter, the tether width, w , which can also be employed, to a second order, to set the center frequency of the acoustic band gap.

The IABG structure was designed and demonstrated in aluminum nitride (AlN). Top and bottom platinum (Pt) layers were introduced to sandwich the AlN film with the purpose of eliminating the reflections induced by the acoustic mismatch between the contour-mode (CM) transducers used to launch and sense acoustic waves and the IABG array (Fig. 2).

COMSOL[®] finite element method (FEM) multiphysics software was used to design the IABG structure for the fre-

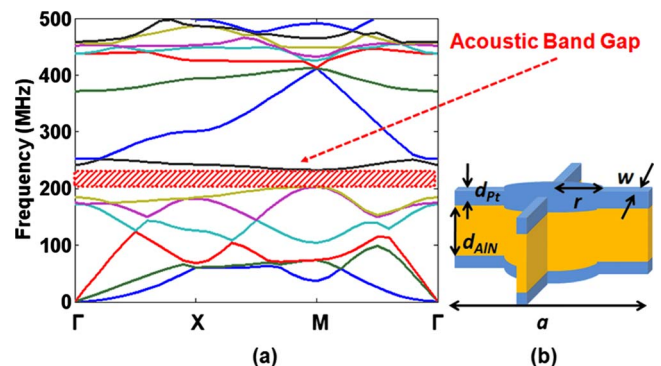


FIG. 1. (Color online) (a) The IABG frequency dispersion relationship simulated via COMSOL[®] FEM. (b) IABG unit cell and its key geometrical parameters.

^{a)} Authors to whom correspondence should be addressed. Electronic addresses: kuo1@seas.upenn.edu, czuo@seas.upenn.edu, and piazza@seas.upenn.edu.

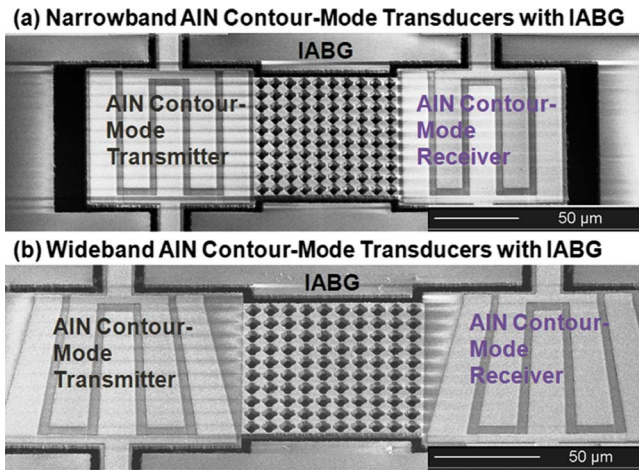


FIG. 2. (Color online) Microfabricated IABG structure coupled by AIN piezoelectric (a) narrowband and (b) wideband contour-mode transducers.

quency range of interest. This approach had been demonstrated and previously validated by Gorishnyy *et al.*⁸ The acoustic wave traveling inside the periodic media is described by the elastic wave equation and the Bloch–Floquet theorem.⁹ In the FEM structural analysis, the eigenfrequencies of the ABG are found by solving the elastic wave equation with periodic boundary conditions applied on the unit cell. Furthermore, the frequency band gap is revealed by sweeping the eigenfrequency solver over the symmetric directions of the first Brillouin zone (Γ - X - M - Γ) of the reciprocal lattice.¹⁰

For operation at 218 MHz, the dimensions of the structure are $a=8.6\ \mu\text{m}$, $r=3.3\ \mu\text{m}$, $w=1\ \mu\text{m}$, $d_{\text{AIN}}=2\ \mu\text{m}$, and $d_{\text{Pt}}=200\ \text{nm}$. The lattice constant, a , sets, to first order, the center frequency. The films thicknesses are constrained by the need of integrating the IABG within the same plane of existing electroacoustic transducers based on the AIN CM technology. An r/a ratio of 0.38 was used to maximize the size of the band gap. The FEM analysis also showed that the band gap width increases inversely with the size of the tether width. Ultimately, in this demonstration, the value of w was limited to $1\ \mu\text{m}$ because of manufacturing limitations. This specific IABG structure in deed generates a complete frequency stop band with a gap-to-midgap ratio of 13.5% and using a thickness to lattice constant (d/a) ratio of just 0.23. The conventional ABG arrangement would have not yielded a measurable band gap for the same d/a .

In this demonstration, two types of transducers are employed to launch in-plane bulk acoustic waves into the IABG structure: narrowband and wideband piezoelectric CM transducers. The design of these transducers is based on the AIN piezoelectric CM technology.¹¹ By means of an electric field applied across the AIN thickness, lateral vibrations are induced via the equivalent d_{31} piezoelectric coefficient. The operating frequency is determined by the device width. A set of transducers consist of two AIN CM resonators: one that launches bulk acoustic waves into the IABG structure, and a second one that receives the acoustic energy and transforms it into an electrical signal (Fig. 2). Thus, in this way, in-plane bulk acoustic waves generated by one transducer propagate inside the IABG structure and are picked-off by the other.

The usable bandwidth of narrowband AIN CM transducers is currently limited by the electromechanical coupling

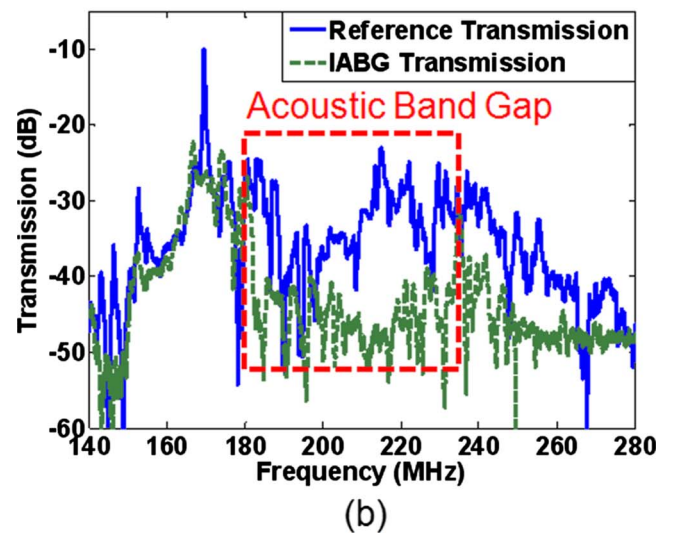
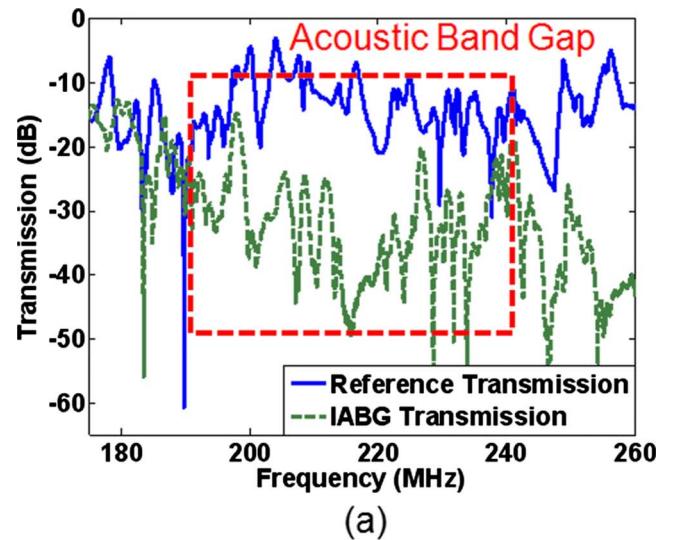


FIG. 3. (Color online) The transmission responses of the IABG structure (green-dotted line) and the reference (blue line) using a (a) eight narrowband transducers set and (b) a single set of wideband transducers.

coefficient, k_r^2 , of AIN to be approximately 4%–5% of the device center frequency and requires that at least eight sets of narrowband CM transducers are fabricated to demonstrate the operation of the frequency stop band. On the other hand, the CM wideband transducers can cover a wider frequency range (at the expenses of a reduced signal intensity) by using a slanted finger technique, similar to what has been demonstrated in surface acoustic wave devices.¹² The wideband transducers eliminate the need of fabricating many copies of the same IABG and reduce potential measurement inaccuracies introduced by fabrication mismatch between the various IABGs (a single IABG is in fact used with the wideband transducers).

The IABG structure was fabricated in the same plane of the AIN CM transducers by means of a four-mask and post-CMOS compatible microfabrication process.¹³ In addition, the same set of transducers coupled to a single plate of AIN sandwiched between Pt layers was also fabricated to operate as a reference for the transmission response of the IABG.

The transmission response of the IABG structure was measured via an Agilent N5230 PNA-L network analyzer after performing a standard short-open-load-through calibra-

tion. The extracted data from the IABG structure were further impedance-matched together with the reference data to reduce electrical losses and almost exclusively emphasize the acoustic characteristics of the device. For the narrowband transducers, 4%–5% bandwidth of the center frequency of each transmission response was taken and added up to cover the entire frequency range of interest. On the other hand, only one set of transducers were required for the IABG demonstration with wideband devices.

The transmission response from both types of transducer verified that the frequency band gap occurs between 185 MHz and 240 MHz and is centered at 218 MHz (Fig. 3). Although the frequency band gap has been demonstrated, the experimental data show a larger stop band than the simulated result (Fig. 1) with additional rejection occurring at higher frequencies. This is due to the fact that the CM devices primarily induce bulk acoustic waves propagating in the [100] direction (Γ - X in Fig. 1). If this is taken into account, then a wider band gap should be expected as shown by the simulated results in the Γ - X direction.

To summarize, this work can be considered a preliminary demonstration of a microscale IABG in AlN. By using an unconventional unit cell topology formed by a high acoustic velocity material in a low acoustic velocity matrix, a wide frequency stop band was attained in microscale AlN structures. The IABG structure was also directly integrated with CM MEMS technology, which was used to synthesize the electroacoustic transducers. This work lays the foundation for future developments aimed at realizing PC-based rf devices such as waveguides, resonators, and filters. Future work will also focus on improving the fabrication process of the IABG structure for obtaining an improved band gap re-

sponse and demonstrate its possible application in the ultra high frequency range (>1 GHz).

The authors would like to thank Tegal Corporation for the AlN deposition and the assistance from the staff of the Wolf Nanofabrication Facility (WNF) at the University of Pennsylvania.

- ¹R. H. Olsson III and I. El-Kady, *Meas. Sci. Technol.* **20**, 012002 (2009).
- ²S. Mohammadi, A. A. Eftekhar, W. D. Hunt, and A. Adibi, *Appl. Phys. Lett.* **94**, 051906 (2009).
- ³A. Khelif, B. Aoubiza, S. Mohammadi, A. Adibi, and V. Laude, *Phys. Rev. E* **74**, 046610 (2006).
- ⁴S. Mohammadi, A. A. Eftekhar, A. Khelif, H. Moubchir, R. Westafer, W. D. Hunt, and A. Adibi, *Electron. Lett.* **43**, 898 (2007).
- ⁵S. Mohammadi, A. A. Eftekhar, A. Khelif, W. D. Hunt, and A. Adibi, *Appl. Phys. Lett.* **92**, 221905 (2008).
- ⁶R. H. Olsson III, J. G. Fleming, I. El-Kady, M. R. Tuck, and F. McCormick, International Conference on Solid-State Sensors, Actuators, and Microsystems TRANSDUCERS 2007, Lyon, France, 2007, pp. 317–321.
- ⁷C. Zuo, N. Sinha, C. R. Perez, R. Mahameed, M. B. Pisani, and G. Piazza, Workshop on Solid-State Sensors, Actuators, and Microsystems, Hilton Head Island, South Carolina, 2008, pp. 324–327.
- ⁸T. Gorishnyy, C. K. Ullal, M. Maldovan, G. Fytas, and E. L. Thomas, *Phys. Rev. Lett.* **94**, 115501 (2005).
- ⁹P. Langlet, A.-C. Hladky-Hennion, and J.-N. Decarpigny, *J. Acoust. Soc. Am.* **98**, 2792 (1995).
- ¹⁰C. Kittel, *Introduction to Solid State Physics* (Wiley, New Jersey, 2005).
- ¹¹G. Piazza, P. J. Stephanou, and A. P. Pisano, Proceeding of 32th European Conference on Solid-State Circuits, Montreux, Switzerland, 2006, pp. 62–65.
- ¹²C.-M. Lin, Y.-Y. Chen, and T.-T. Wu, *J. Phys. D: Appl. Phys.* **39**, 466 (2006).
- ¹³N. Sinha, R. Mahameed, C. Zuo, M. B. Pisani, C. R. Perez, and G. Piazza, Workshop on Solid-State Sensors, Actuators, and Microsystems, Hilton Head Island, South Carolina, 2008, pp. 22–25.